Hindawi
Shock and Vibration
Volume 2021, Article ID 9059228, 12 pages
https://doi.org/10.1155/2021/9059228

*Research Article*

# Experimental Study on Mudstone's Strength Characteristics in Deep-Buried Coal-Measure Formation: A Case Study of Permian Longtan Formation

**Ke Li**,[1,2] **Weijian Yu**,[1,3] **Youlin Xu**,[2] **Long Lai**,[4] **Hui Zhang**,[2] **Mengtang Xu**,[2] **and Ze Zhou**[2]

[1]*School of Resource & Environment and Safety Engineering, Hunan University of Science and Technology, Xiangtan, Hunan 411201, China*
[2]*College of Mining, Guizhou Institute of Technology, Guiyang, Guizhou 550003, China*
[3]*Hunan Provincial Key Laboratory of Safe Mining Techniques of Coal Mines, Hunan University of Science and Technology, Xiangtan, Hunan 411201, China*
[4]*Guizhou Panjiang Coal and Electricity Group Co. Ltd., Panzhou, Guizhou 553599, China*

Correspondence should be addressed to Ke Li; 20120016@git.edu.cn

Received 30 August 2021; Revised 24 September 2021; Accepted 12 October 2021; Published 1 November 2021

Academic Editor: Lishuai Jiang



To investigate the strength characteristics of mudstone in deep-buried coal-measure formation, four types of experiments have been conducted: (i) the X-ray diffraction (XRD) test; (ii) the scanning electron microscope (SEM) scanning test; (iii) the point load strength index test; and (iv) the uniaxial compressive strength test. It was concluded that the mudstone of the deep-buried coal measures in the Longtan Formation is dominated by chlorite, quartz, and albite using the XRD test, of which chlorite is primary, accounting for 74.3%. It was found that the three minerals in the mudstone are unevenly distributed using the SEM scanning test, albite is irregularly distributed in chlorite, and quartz is present in the albite and chlorite. Sixty-five specimens were tested for the point load strength index. After processing the data using the method suggested by the International Society for Rock Mechanics and Rock Engineering(ISRM), it was found that the maximum value of $I_{s(50)}$ was 6.10 MPa, the minimum is 0.14 MPa, and 53% of the specimens' $I_{s(50)}$ values are below 2.0 MPa. The RMT-150C rock mechanics testing machine was used to conduct uniaxial compression tests on six specimens. The maximum uniaxial compressive strength (UCS) value is 59.26 MPa, the minimum value is 31.77 MPa, and the average is 45.64 MPa. Linear fitting and logarithmic fitting are carried out for the correlation between UCS and $I_{s(50)}$. The goodness of fit $R^2$ of the linear fitting is 0.863, and that of the logarithmic fitting is 0.919, indicating a strong correlation between them. When it is challenging to make standard specimens, $I_{s\ (50)}$ can be used to estimate UCS.

## 1. Introduction

UCS of deep-buried coal-measure formation is an important index to evaluate its stability and an essential reference basis for arranging roadway system and selecting mining technology [1–3]. Generally, the rock depositional environment of deep-buried coal-measure formation is complex and cooccurs with coal seams, resulting in a complex composition, high heterogeneity, and a high degree of joint and fissure development, which significantly reduces the integrity and strength of coal-measure formation [4–6]. According to the suggested method of ISRM, there are strict requirements for the specimen when testing UCS. The most basic requirement is that the length/diameter ratio of the specimen is greater than 2 [7, 8]. However, in the field sampling with a high fracture development program or high degree of rock fragmentation, it is challenging to obtain a complete core for routine UCS tests in many cases.

Andrea and Fisher [9] first used the point load test to estimate the uniaxial compressive strength of rock and considered a linear relationship between them. Broch and Franklin [10] considered that the index could be obtained

whatever the shape of the specimen is, and the point load strength results correlated closely with those from uniaxial (unconfined) compressive strength testing. ISRM [7] published "Suggested method for determining point load strength" in 1972 and revised it in 1985. The American Society for Testing and Materials (ASTM) [11] released the standard test method for testing the point load strength index in 1995 and revised it in 2016. In the past 50 years, there has been many research works on the point load strength test. Ulusay and Türeli [12] considered that the point load test is most importantly employed in estimating the compressive strength of rock materials. Bieniawski [13] discussed the practical applications of the point load test in geotechnical practice and proposed that the diametral point load test is most convenient and reliable in use. Broch [14] considered that the most reliable point load strength index would be obtained when cores are drilled normal or near-normal to weakness planes. Brook [15] considered that the general usefulness of the point load strength test was applying compressive strength estimation, rock mass classification, estimation of triaxial behavior, and small-scale physical model testing. Şahin et al. [16] studied the point load strength index of half-cut core specimens and its correlation with uniaxial compressive strength. Fan et al. [17] considered that the distance between two loading points and the width of the actual fracture section played an essential and nonnegligible role for the failure of rock specimens. Lei et al. [18] proposed that there is no significant difference in the shape distribution with the block size. Sha [19] considered that the fitting equations could align with reality for relatively hard and homogeneous rocks.

The relationship between the point load strength index and UCS is the focus of the point load test. In recent years, there are many reports on the relationship between them, which are aimed at different types of rocks. ISRM [7], Forster [20], Ghosh and Srivastava [21], Chau and Wong [22], Smith [23], Tsiambaos and Sabatakakis [24], Palchik and Hatzor [25], Singh et al. [26], Kohno and Maeda [27], Li and Wong [28], Şahin et al. [16], Kaya and Karaman [29], Liu et al. [30], Rabat et al. [31], Xue et al. [32], and Xie et al. [33] considered that the two were linear with zero intercept. Andrea et al. [9], Ulusay et al. [12], Kahrama [34], Diamantis et al. [35], Yilmaz [36], Kaya and Karaman [29], Heidari et al. [37], and Kong and Shang [38] et al. believed that the two are linear relations of non-zero intercept. Kahraman [34], Tsiambaos and Sabatakakis [24], Santi [39], Selçuk and Süleyman Gökçe [40], and Kallu and Roghanchi [41] considered the two to be a power function relationship. Kılıç and Teymen [42] considered the two to be a logarithmic function relationship. Quane and Russell [43] considered the two to be a quadratic function relationship. Their research is aimed at different rocks, and the expressions are fitted according to the laboratory test results. They have reference value for specific rocks in a certain range. That is, targeted research is needed for specific rocks to obtain applicable expressions.

This study conducted XRD test, SEM scanning test, point load test, and uniaxial compression test in the laboratory to study the strength characteristics of mudstone in deep-buried coal-measure strata in detail. Their strength characteristics were analyzed, and the possibility of replacing the uniaxial compression test with point load test was studied, to provide references for scientific decisions such as arranging roadways, selecting support methods, and selecting mining engineering.

## 2. Main Composition and Structure of the Rock Specimens

*2.1. Sample Source.* The specimens in this research are from the Huopu coal mine in Panzhou City, Guizhou Province, a province in southwest China. The specimens are taken from the rock formation between the 23# and 24# coal seams of this coal mine. The distance between the two coal layers is 14.3 m. The buried depth of the specimens is 1349 m-1355 m, the specimen diameter is 50 mm, and the primary lithology is thin dark gray mudstone. The rock cores drilled on-site are shown in Figure 1, and the statistics show that its RQD value is only 28.9%.

*2.2. XRD Test.* To analyze the mineral composition of mudstone, Uitima IV X-ray diffractometer is used to study mudstone specimens. The inspection results are shown in Figure 2. According to "general rules for X-ray polycrystalline diffraction" (A Chinese technical specification, designation: JY/T 0587-2020) [44], the experimental results are processed by the adiabatic quantitative method. It can be seen that the mudstone is mainly composed of chlorite, quartz, and albite, of which chlorite accounts for 74.3%. Chlorite is a clay mineral, which loosens easily when exposed to water. The quantitative test results of mineral composition are shown in Table 1.

*2.3. Observation of Rock Fracture Morphology.* To observe the detailed structure of the rock, a Nova Nano SEM 450 hot field emission scanning electron microscope was used to scan the surface of the rock after fracture, and SEM images with different magnification were obtained, as shown in Figure 3. From these SEM images, it can be seen that the microcracks extending from the rock surface to the content are extremely developed. PCAS software is used to analyze the pore data in 500 times SEM images, as shown in Figure 4. The calculated surface porosity is 3.01%. The number of pores directly affects the mechanical properties of rock. As the proportion of rock's pores increases, the strength of the rock becomes lower.

It can be seen from Figure 3 that the distribution of various mineral components in the mudstone is uneven, albite is distributed irregularly in chlorite in blocks, and quartz occurs in spots in albite and chlorite, showing substantial heterogeneity.

The wide distribution of pores and fractures in mudstone and its heterogeneity reduce its strength to a great extent, which is why it is difficult to obtain a complete core during field sampling.

Figure 1: Samples of field borehole sampling.

## 3. Point Load Strength Index Test and Results Analysis

*3.1. Point Load Strength Index Test.* After processing the specimens in Figures 1, 6 specimens for uniaxial compression and 65 specimens for point load test are obtained. The specimens before the test are shown in Figure 5(a). The experimental instrument is the STDZ-3 point load tester. There were 46 valid tests and 19 invalid ones. There were three reasons for the invalid tests: firstly, some samples only damaged one corner, which belongs to the invalid test specified by ISRM [7]. Secondly, some specimens are broken into massive rocks after testing, and their failure surface cannot be measured. Thirdly, some specimens have internal cracks, which are not observed on the surface, which significantly reduce their strength and destroy the test so fast that the instrument cannot effectively monitor the failure load. That is, there are no valid test data in these tests. The specimens after the test are shown in Figure 5(b). The test results are shown in Table 2.

*3.2. Experimental Data Processing.* According to the suggested method of ISRM [7], the point load test data can be processed with the following equation:

$$\begin{cases} I_{S(50)} = F \times I_S, \\ I_S = \dfrac{P}{D_e^2}, \\ D_e = \left(\dfrac{4A}{\pi}\right)^{0.5}, \\ A = W \times D, \\ F = \left(\dfrac{D_e}{50}\right)^{0.45}, \end{cases} \tag{1}$$

where $I_{S(50)}$ is the modified point load strength, MPa. $I_S$ is the unmodified point load strength, MPa. $F$ is the size modification factor. $P$ is the point load strength, kN. $D_e$ is the equivalent core diameter, mm. $A$ is the damaged area, mm$^2$. $W$ is the width of the damaged surface, mm. and $D$ is the height of the damaged surface, mm.

In addition, when the rock is damaged, the spacing between loading points is generally not equal to $D$, but it is damaged after being pressed into the rock for a short distance. Therefore, ASTM D5731-16 [11] and other technical standards proposed that if significant plate penetration occurs in the test, such as when testing weak sandstones, the value of $D$ should be the final value of the separation of the loading points, $D'$. during the experiment in this study, it is found that significant platen penetration often occurs, as shown in Figure 6. Therefore, when processing the test data in this study, the specimens of significant platen penetration are calculated by $D'$, and others are calculated by $D$.

Sorting out equation (1), the point load strength calculation equation of the specimen without significant platen penetration is

$$I_{S(50)} = \frac{P}{50^{0.45}} \cdot \left(\frac{\pi}{4WD}\right)^{0.775}. \tag{2}$$

The calculation equation of the point load strength of the specimen with significant platen penetration is

$$I_{S(50)} = \frac{P}{50^{0.45}} \cdot \left(\frac{\pi}{4WD'}\right)^{0.775}. \tag{3}$$

Using equations (2) and (3) to process the experimental data, $I_{s(50)}$ is obtained, as shown in Table 2. In addition, according to the suggested method of ISRM, each group of data should delete the two maximum values and two minimum values and then take the average of the other values as the $I_{s(50)}$ of the group of experiments. The number of successes in each group of experiments in this study is less than 10, so this study only deletes a maximum value and a minimum value of each group, and the average value of $I_{s(50)}$ for each group is shown in Table 2.

According to the above test results, before removing the extreme value, among the 46 tests, the maximum value of $I_{s(50)}$ is 6.10 MPa, and the minimum value is 0.14 MPa. The statistical distribution range is shown in Figure 7(a). It can be seen that, among the 46 data, 24 have $I_{s(50)}$ below 2.0 MPa, accounting for 53% of the total, and 17 have $I_{s(50)}$ below 1.0 MPa, accounting for 37% of the total. Remove a maximum value and a minimum value for each group. That is, after removing the data of 12 specimens, among the 34 tests, the maximum value of $I_{s(50)}$ is 4.19 MPa, and the minimum value is 0.25 MPa. The statistical distribution range is shown in Figure 7(b).

## 4. Uniaxial Compression Test

*4.1. Test Methods and Equipment.* The test specimen is from the core in Figure 1. Because the rock is very broken, only six specimens are obtained, and the length of these specimens is less than 100 mm. After the specimens were cut by the cutting machine, the TX-SHM200 C program-controlled double-ends planishing machine was used for polish. After the specimen is ground flat, the ends of the specimens were flat to 0.02 mm and were moved from permanency to the axis of the specimens by less than 0.05 mm.

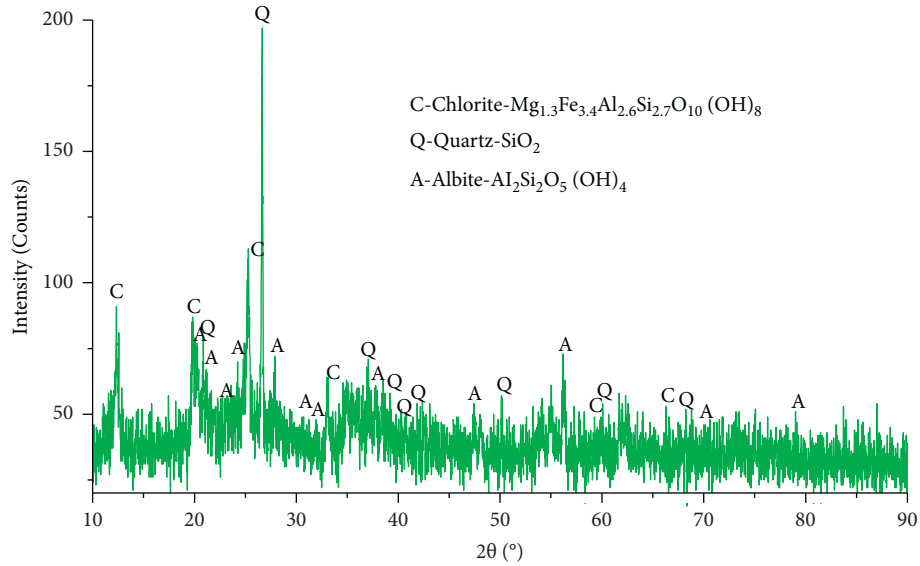


Figure 2: XRD pattern of mudstone.

Table 1: The quantitative test results of mineral composition.

| No. | Mineral name | Chemical formula | Mineral content accounted (%) |
|---|---|---|---|
| 1 | Chlorite | $Mg_{1.3}Fe_{3.4}Al_{2.6}Si_{2.7}O_{10}(OH)_8$ | 74.3 |
| 2 | Quartz | $SiO_2$ | 16.2 |
| 3 | Albite | $NaAlSi_3O_8$ | 9.5 |

The uniaxial compression test was carried out in the Mechanical Laboratory of Hunan University of Science and Technology. The loading equipment is a RMT-150C rock mechanics testing machine. DH3816 N static strain tester and wire-wound resistor were used for deformation monitoring. The test system is shown in Figure 8.

Linear incremental force loading control is adopted, and the loading rate is 1 kN/s, that is, 0.5 MPa/s. When the test piece is damaged, the pressure head of the loading system will return automatically. Each specimen is pasted with four strain gauges, two to monitor axial deformation and two to monitor radial deformation. The average value is taken as the axial and radial deformation value, respectively. DH3816 N static strain tester is used to monitor the deformation data of the specimen in real-time during loading.

*4.2. Test Results.* The test data of 6 specimens are shown in Table 3, and the uniaxial compressive stress-strain data of 6 specimens are shown in Figure 9. Among the six specimens, the largest UCS is 59.26 MPa, the smallest is 31.77 MPa, and the average value is 45.64 MPa. The results of each specimen are quite different. It is speculated that the reason is that the distribution of chlorite, quartz, and albite minerals in the specimen is not uniform, resulting in a high degree of heterogeneity in the specimen, resulting in a significant difference in UCS.

It can be seen from Figure 9 that the strain of each specimen is slight in the early stage of loading. That is, it is not apparent in the compaction stage, and the rock shows obvious brittleness.

*4.3. Data Correction.* ASTM [45] suggested an equation to convert UCS values of test specimens having an $L/D$ ratio less than 2 : 1 to that of a specimen with a ratio of 2 : 1 (equation (4)):

$$UCS_2 = \frac{UCS}{(0.88 + 0.24D/L)}, \quad (4)$$

where $UCS_2$ is the corrected value for a $L/D$ ratio of 2 : 1, $L$ is the length of the specimen, and $D$ is the diameter of the specimen, while the UCS is the measured value on cores with a $L/D$ ratio less than 2 : 1.

Equation (4) can be used to convert the UCS values of specimens with $L/D$ ratios <2 to a standard ratio, which is accepted as 2. The revised data using equation (4) is shown in Table 3.

## 5. Correlation between UCS and $I_{s(50)}$

The average $I_{s(50)}$ of the 46 specimens tested in this study is 2.11 MPa, the revised average $USC_2$ is 44.26 MPa, and the ratio of the two is 21.0, which is very close to the ratio of 24 given by ISRM [7], and many reported that the relationship between the point load strength index and UCS is a linear relationship with zero intercepts. To further qualitatively and quantitatively characterize the relationship between UCS and $I_{s(50)}$ of deep-buried coal-measure formation mudstone, based

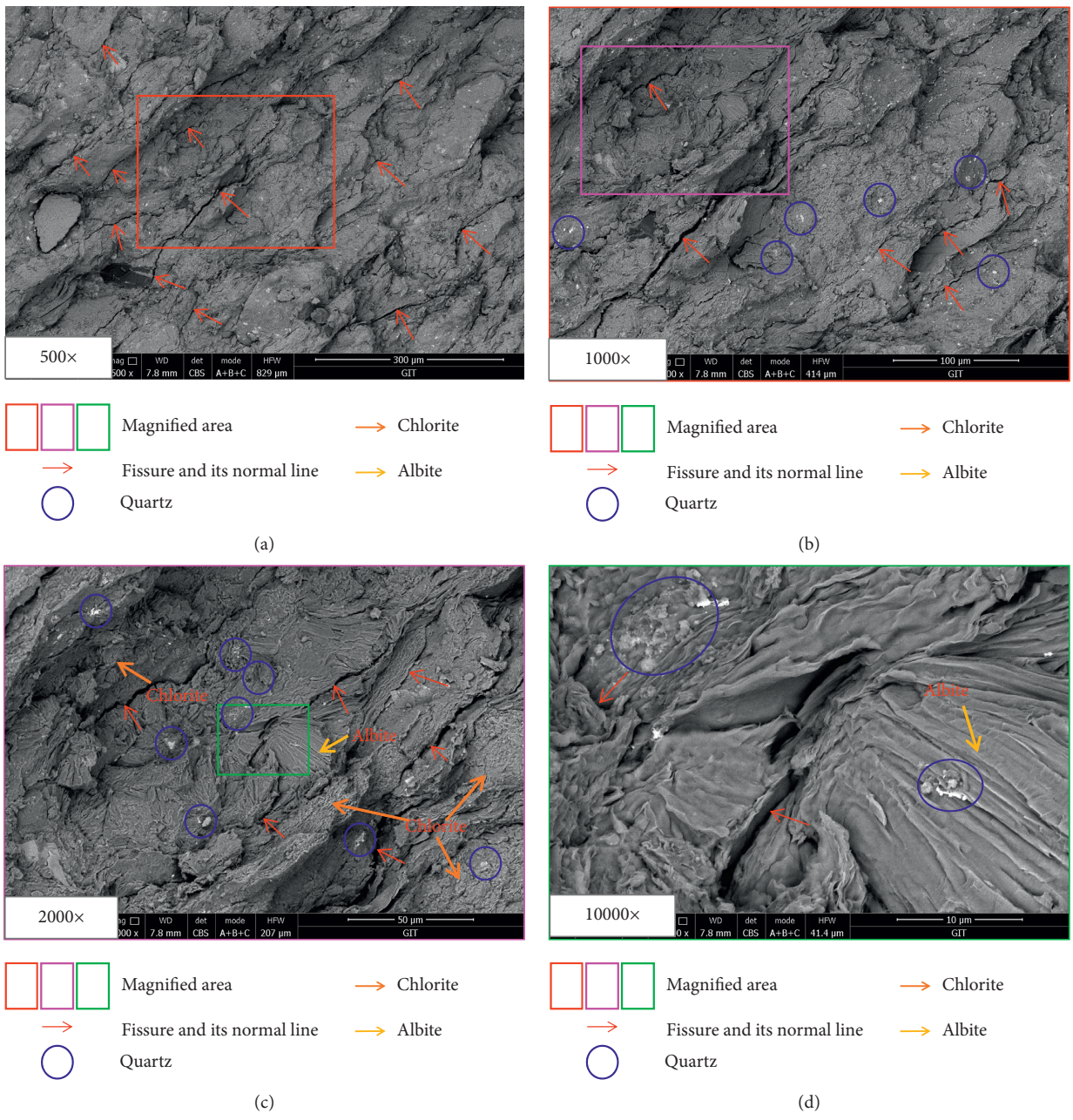


Figure 3: SEM images of mudstone.

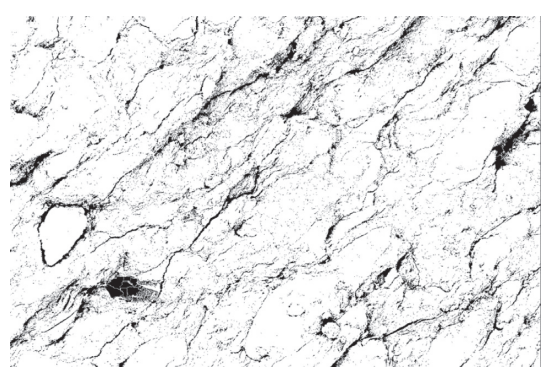

Figure 4: Pore distribution on the specimen surface.

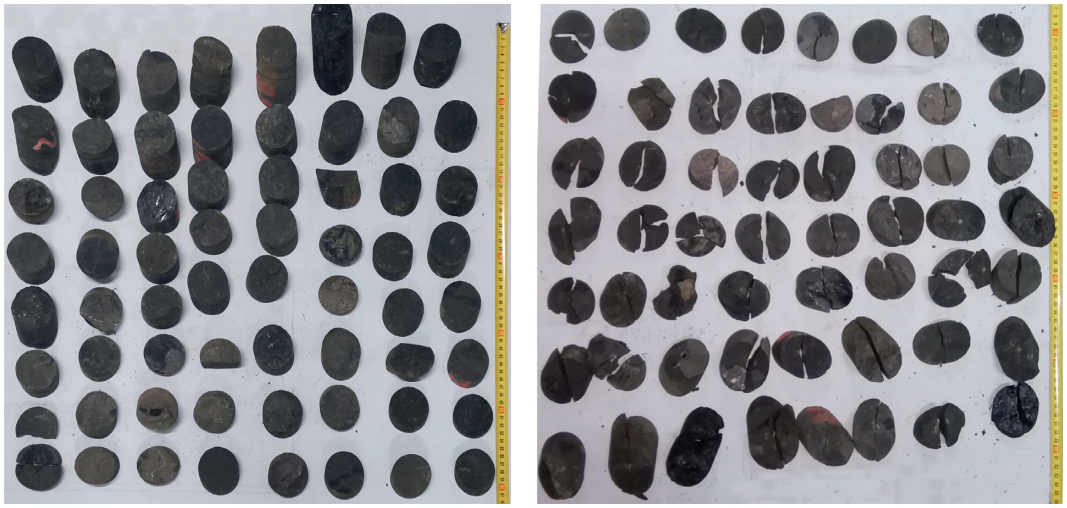

(a) (b)

Figure 5: Specimens before and after point load test. (a) Before test. (b) After test.

Table 2: Point load test results.

| Group no. | Specimen no. | $W$ (mm) | $D$ (mm) | $D'$ (mm) | $P$ (N) | $A$ (mm$^2$) | $D_e$ (mm) | $I_s$ (MPa) | $F$ | $I_{s(50)}$ (MPa) | Mean value (MPa) |
|---|---|---|---|---|---|---|---|---|---|---|---|
| | *1a1* | 45.18 | 16.88 | 14.02 | 260 | 633.35 | 28.40 | 0.32 | 0.78 | 0.25 | |
| | *1a2* | 52.64 | 16.96 | 11.81 | 3210 | 621.62 | 28.13 | 4.06 | 0.77 | 3.13 | |
| | *1a3* | 49.79 | 5.72 | | 1410 | 284.80 | 19.04 | 3.89 | 0.65 | 2.52 | |
| | *1a4* | 51.55 | 13.20 | 9.98 | 1530 | 514.47 | 25.59 | 2.34 | 0.74 | 1.73 | |
| 1 | *1a5* | 54.46 | 18.54 | 15.04 | 860 | 819.08 | 32.29 | 0.82 | 0.82 | 0.68 | 1.82 |
| | *1a6* | 51.50 | 18.62 | | 370 | 958.93 | 34.94 | 0.30 | 0.85 | 0.26 | |
| | *1a7* | 48.69 | 15.65 | 11.12 | 5230 | 541.43 | 26.26 | 7.59 | 0.75 | 5.68 | |
| | *1a8* | 49.96 | 15.51 | 11.84 | 4120 | 591.53 | 27.44 | 5.47 | 0.76 | 4.18 | |
| | *1a9* | 47.36 | 28.01 | | 258 | 1326.55 | 41.10 | 0.15 | 0.92 | 0.14 | |
| | *2a1* | 49.32 | 13.74 | 9.09 | 3830 | 448.32 | 23.89 | 6.71 | 0.72 | 4.81 | |
| | *2a2* | 49.44 | 16.33 | | 750 | 807.36 | 32.06 | 0.73 | 0.82 | 0.60 | |
| | *2a3* | 50.54 | 10.14 | 5.43 | 310 | 274.43 | 18.69 | 0.89 | 0.64 | 0.57 | |
| | *2a4* | 47.84 | 23.46 | 19.19 | 390 | 918.05 | 34.19 | 0.33 | 0.84 | 0.28 | |
| 2 | *2a5* | 47.03 | 26.61 | | 2910 | 1251.47 | 39.92 | 1.83 | 0.90 | 1.65 | 1.60 |
| | *2a6* | 48.87 | 20.18 | 13.84 | 2340 | 676.36 | 29.35 | 2.72 | 0.79 | 2.14 | |
| | *2a7* | 51.21 | 15.78 | | 1310 | 808.09 | 32.08 | 1.27 | 0.82 | 1.04 | |
| | *2a8* | 53.64 | 16.61 | 11.9 | 3740 | 638.32 | 28.51 | 4.60 | 0.78 | 3.57 | |
| | *3a1* | 52.55 | 20.73 | 16.73 | 3710 | 879.16 | 33.46 | 3.31 | 0.83 | 2.77 | |
| | *3a2* | 53.50 | 16.37 | 10.3 | 1340 | 551.05 | 26.49 | 1.91 | 0.75 | 1.43 | |
| | *3a3* | 48.76 | 18.60 | 12.69 | 4670 | 618.76 | 28.07 | 5.93 | 0.77 | 4.57 | |
| 3 | *3a4* | 53.27 | 25.08 | | 780 | 1336.01 | 41.24 | 0.46 | 0.92 | 0.42 | 1.48 |
| | *3a5* | 49.83 | 21.31 | | 1040 | 1061.88 | 36.77 | 0.77 | 0.87 | 0.67 | |
| | *3a6* | 50.15 | 29.54 | | 470 | 1481.43 | 43.43 | 0.25 | 0.94 | 0.23 | |
| | *3a7* | 50.62 | 26.61 | | 3910 | 1347.00 | 41.41 | 2.28 | 0.92 | 2.09 | |
| | *4a1* | 48.71 | 28.14 | 22.19 | 4340 | 1080.87 | 37.10 | 3.15 | 0.87 | 2.76 | |
| | *4a2* | 49.92 | 24.46 | 20.14 | 3610 | 1005.39 | 35.78 | 2.82 | 0.86 | 2.43 | |
| | *4a3* | 45.52 | 18.72 | 12.98 | 6010 | 590.85 | 27.43 | 7.99 | 0.76 | 6.10 | |
| | *4a4* | 47.12 | 22.68 | | 510 | 1068.68 | 36.89 | 0.37 | 0.87 | 0.33 | |
| 4 | *4a5* | 49.28 | 25.53 | 20.65 | 4230 | 1017.63 | 36.00 | 3.26 | 0.86 | 2.82 | 2.16 |
| | *4a6* | 45.08 | 34.14 | | 1530 | 1539.03 | 44.27 | 0.78 | 0.95 | 0.74 | |
| | *4a7* | 47.23 | 25.01 | | 5200 | 1181.22 | 38.78 | 3.46 | 0.89 | 3.08 | |
| | *4a8* | 48.18 | 32.83 | 27.45 | 2110 | 1322.54 | 41.04 | 1.25 | 0.91 | 1.15 | |

Table 2: Continued.

| Group no. | Specimen no. | $W$ (mm) | $D$ (mm) | $D'$ (mm) | $P$ (N) | $A$ (mm$^2$) | $D_e$ (mm) | $I_s$ (MPa) | $F$ | $I_{s(50)}$ (MPa) | Mean value (MPa) |
|---|---|---|---|---|---|---|---|---|---|---|---|
| 5 | *5a1* | 46.83 | 19.82 | 16.77 | 5170 | 785.34 | 31.62 | 5.17 | 0.81 | 4.21 | 2.58 |
| | *5a2* | 52.11 | 21.01 | | 450 | 1094.73 | 37.33 | 0.32 | 0.88 | 0.28 | |
| | *5a3* | 42.25 | 26.67 | | 5230 | 1126.81 | 37.88 | 3.65 | 0.88 | 3.22 | |
| | *5a4* | 52.37 | 29.73 | 25.1 | 3640 | 1314.49 | 40.91 | 2.17 | 0.91 | 1.99 | |
| | *5a5* | 49.50 | 21.27 | 16.77 | 5370 | 830.12 | 32.51 | 5.08 | 0.82 | 4.19 | |
| | *5a6* | 48.62 | 17.46 | 13.87 | 1030 | 674.36 | 29.30 | 1.20 | 0.79 | 0.94 | |
| 6 | *6a1* | 50.32 | 44.45 | | 630 | 2236.50 | 53.36 | 0.22 | 1.03 | 0.23 | 2.05 |
| | *6a2* | 46.54 | 23.13 | 18.49 | 3420 | 860.52 | 33.10 | 3.12 | 0.83 | 2.59 | |
| | *6a3* | 49.40 | 36.38 | 30.86 | 1570 | 1524.48 | 44.06 | 0.81 | 0.94 | 0.76 | |
| | *6a4* | 48.31 | 28.68 | 21.61 | 7510 | 1043.98 | 36.46 | 5.65 | 0.87 | 4.90 | |
| | *6a5* | 48.68 | 29.58 | 24.45 | 4560 | 1190.23 | 38.93 | 3.01 | 0.89 | 2.69 | |
| | *6a6* | 51.51 | 42.85 | | 9630 | 2206.99 | 53.01 | 3.43 | 1.03 | 3.52 | |
| | *6a7* | 45.75 | 32.92 | | 4010 | 1505.93 | 43.79 | 2.09 | 0.94 | 1.97 | |
| | *6a8* | 54.37 | 18.22 | | 1120 | 990.62 | 35.51 | 0.89 | 0.86 | 0.76 | |

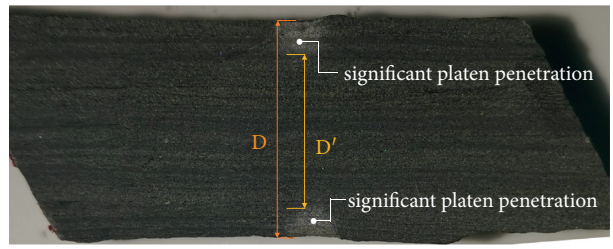


Figure 6: Significant platen penetration.

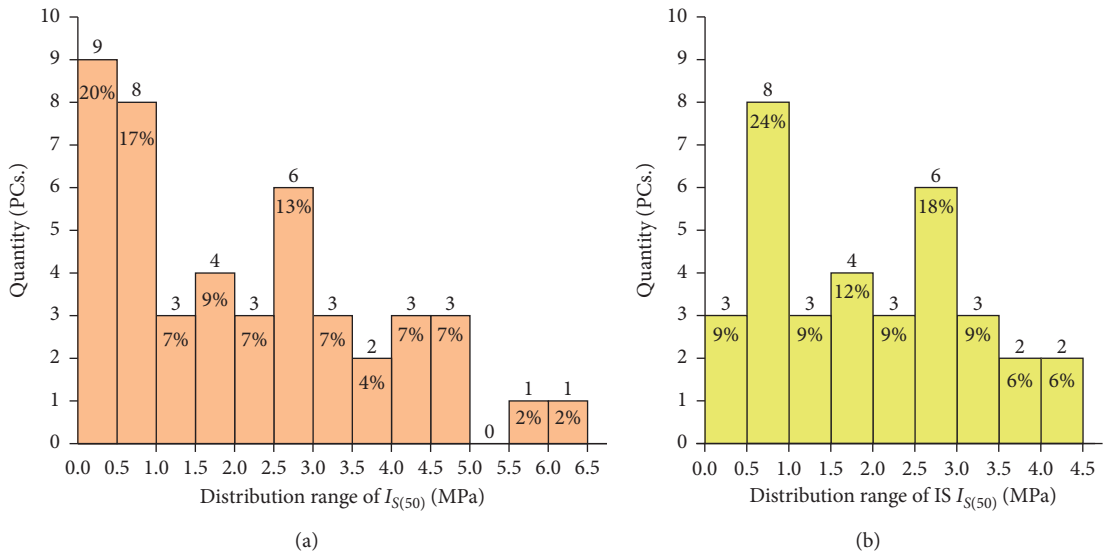


Figure 7: Statistics of point load test results. (a) Before removing the extreme value. (b) After removing the extreme value.

on previous research results, this study performed linear fitting and logarithmic fitting on UCS and $I_{s(50)}$ obtained from the experiment. The results are shown in Figure 10.

It can be seen from Figure 10, within the range of six groups' average $I_{s(50)}$ obtained in this study, there is little difference between ISRM and the three $USC_2$ prediction equations obtained in this study. However, beyond the scope of the results of this study, the result obtained by logarithmic fitting is quite different from those obtained by the other three prediction methods. According to the results of logarithmic fitting, when $I_{s(50)}$ is less than 1.5 MPa, $USC_2$ increases sharply with the increase of $I_{s(50)}$, and their slope is much higher than the linear results. When $I_{s(50)}$ is greater than 3.0 MPa, $USC_2$ increases slowly with the increase of $I_{s(50)}$, and their slope is much lower than the linear results.

It can be seen from the fitting results that the goodness of fit $R^2$ of UCS and $I_{s(50)}$ is 0.863 for linear fitting, and $R^2$ for logarithmic fitting is 0.919, indicating that there is a strong correlation between them. The logarithmic expression is

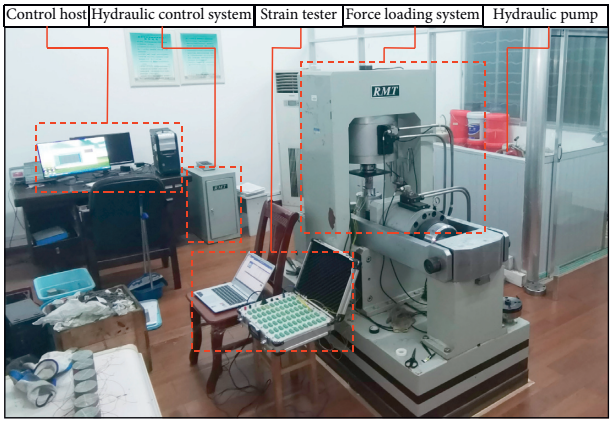


Figure 8: Uniaxial compression test system.

Table 3: Specimens parameters and UCS test results.

| Specimen no. | Length (mm) | Diameter (mm) | Weight (g) | Density (kg/m$^3$) | Load at failure (kN) | UCS (MPa) | $UCS_2$ (MPa) |
|---|---|---|---|---|---|---|---|
| 617 | 53.08 | 48.55 | 253.8 | 2583 | 58.82 | 31.77 | 28.90 |
| 621 | 80.90 | 48.89 | 413.6 | 2724 | 95.84 | 51.05 | 49.81 |
| 622 | 99.42 | 48.63 | 480.4 | 2602 | 99.74 | 53.70 | 53.84 |
| 623 | 80.43 | 48.49 | 417.0 | 2808 | 61.54 | 33.32 | 32.52 |
| 624 | 86.30 | 48.47 | 430.0 | 2700 | 82.58 | 44.75 | 44.10 |
| 625 | 68.36 | 48.73 | 370.4 | 2905 | 110.52 | 59.26 | 56.38 |
| Mean value | | | | 2720 | 84.84 | 45.64 | 44.26 |

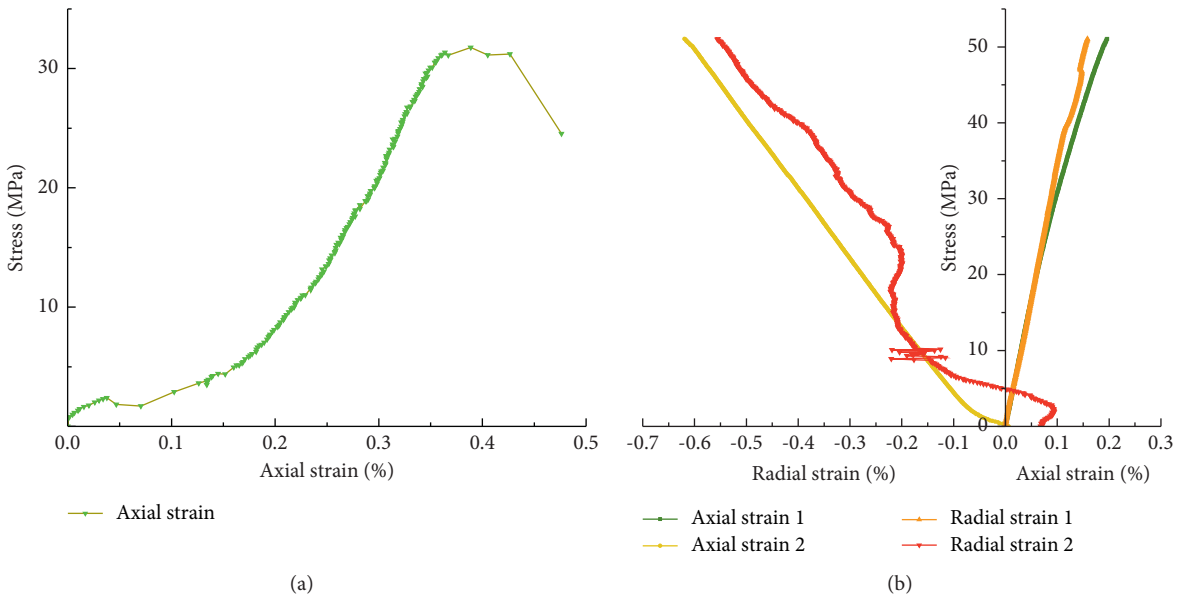


Figure 9: Continued.

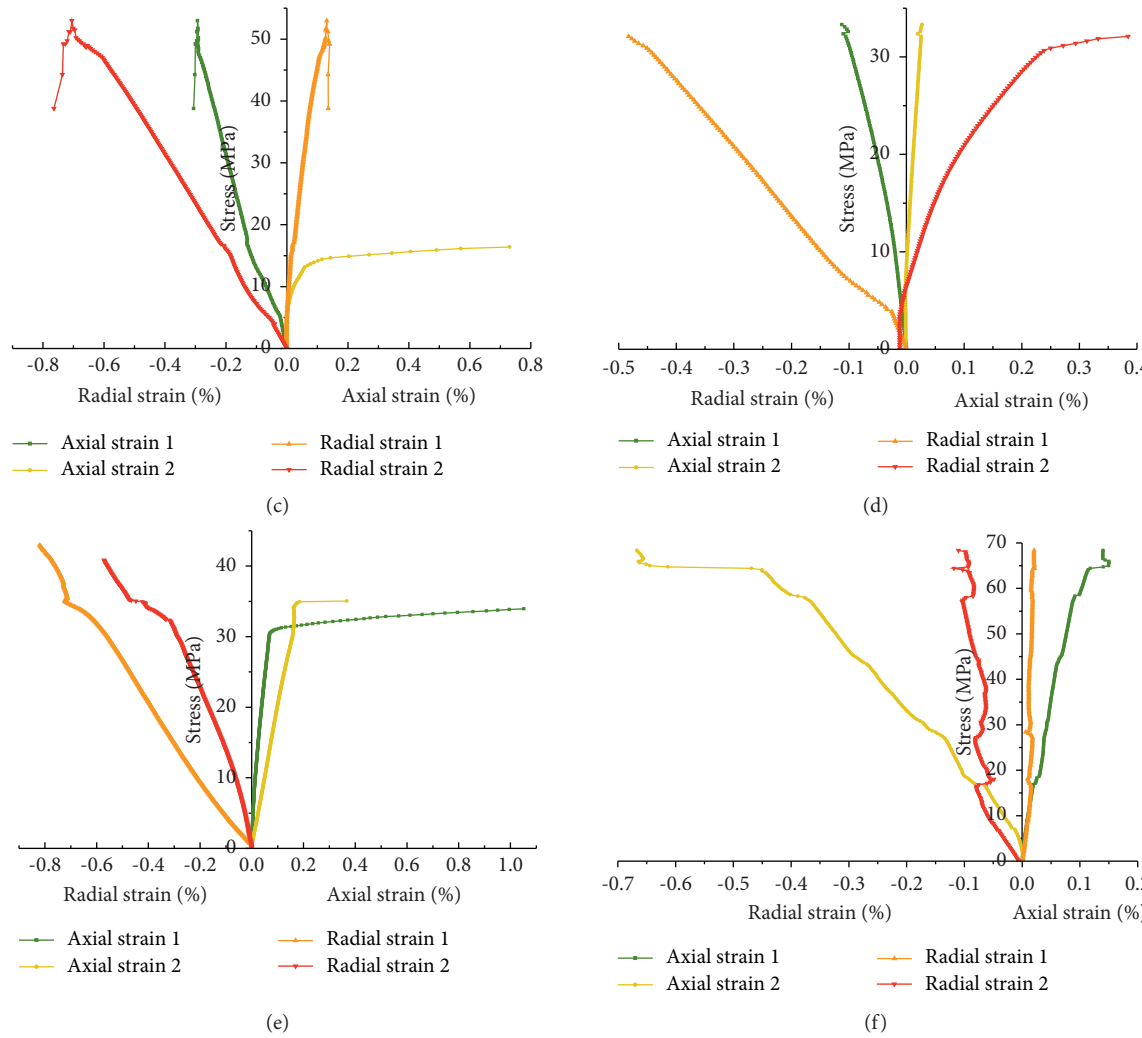


Figure 9: Stress-strain relationships of uniaxial compression test. (a) 617. (b) 621. (c) 622. (d) 623. (e) 624. (f) 625.

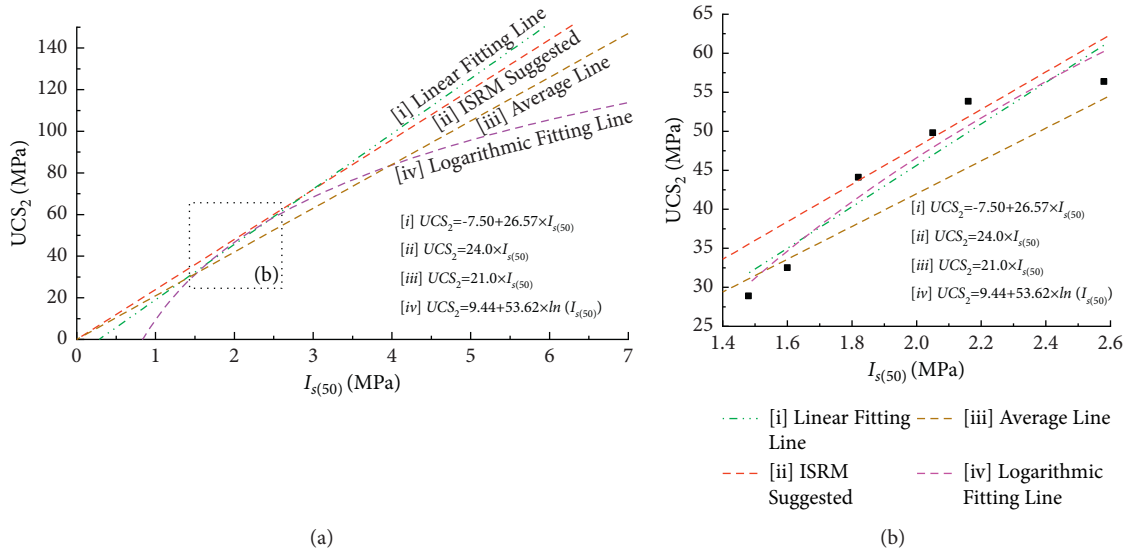


Figure 10: Correlation between USC2 and $I_{s(50)}$. (a) Comparison of ISRM suggested method and results of this study. (b) Partially enlarged figure.

Table 4: UCS and $I_{s(50)}$ fitting parameters.

| Item | Fitting type | Weight | Residual sum of squares | Pearson's r | COD($R^2$) | Adjusted $R^2$ |
|---|---|---|---|---|---|---|
| Value | Linear | No weighting | 70.728 | 0.943 | 0.890 | 0.863 |
| | Logarithmic | — | 10.416 | — | 0.935 | 0.919 |

slightly better than the linear expression. The fitting expression is shown in

$$\begin{aligned} UCS_2 &= \mathrm{a} + b \times I_{S(50)}, \\ UCS_2 &= \mathrm{c} + d \times \ln\left(I_{S(50)}\right), \end{aligned} \tag{5}$$

where a is the linear intercept, $a = -7.50 \pm 9.26$, $b$ is the linear slope, $b = 26.57 \pm 4.67$, and $c$ and $d$ are the logarithmic fitting constants, $c = 9.44 \pm 4.77$, $d = 53.62 \pm 7.06$.

The fitting parameters are shown in Table 4.

## 6. Conclusion

(1) It was concluded that the mudstone of deep-buried coal measures of Longtan Formation is mainly chlorite, quartz, and albite using the XRD test, of which chlorite is the main, accounting for 74.3%. It was found that the three minerals in the mudstone are unevenly distributed using the SEM scanning test, albite is irregularly distributed in chlorite, and quartz is dotted in albite and chlorite, resulting in significant heterogeneity of the mudstone.

(2) Sixty-five specimens were tested for the point load strength index. After processing the data using the method suggested by ISRM, it was found that the maximum value of $I_{s(50)}$ was 6.10 MPa, the minimum is 0.14 MPa, and 53% of the specimens' $I_{s(50)}$ values are below 2.0 MPa.

(3) The uniaxial compression tests of six specimens were carried out in the laboratory using a RMT-150C rock mechanics testing machine. The maximum UCS was 59.26 MPa, the minimum was 31.77 MPa, and the average value was 45.64 MPa. The results of each specimen were quite different. It is speculated that the reason is due to the uneven distribution of chlorite, quartz, and albite minerals in the specimen.

(4) Linear fitting and logarithmic fitting are carried out for the relationship between UCS and $I_{s(50)}$. The goodness of fit $R^2$ of the linear fitting is 0.863, and that of the logarithmic fitting is 0.919, indicating that there is a strong correlation between them. When it is challenging to make standard specimens, Is(50) can be used to estimate UCS.

## Data Availability

The data used to support the findings of this study are included within the article.

## Conflicts of Interest

All the authors declare that they have no known conflicts of interest that could influence the work reported in this paper.

## Acknowledgments

This research was financially supported by National Natural Science Foundation of China (Nos. 51974117 and 52174076), Hunan Provincial Natural Science Foundation of China (No. 2020JJ4027), New Talent Training Project of Guizhou Institute of Technology (No. GZLGXM-02), and Science and Technology Project for Outing and Young Talents of Guizhou (No. QKHPTRC[2019] 5674).

## References

[1] W. J. Yu, G. S. Wu, B. Pan, Q. H. Wu, and Z. Liao, "Experimental investigation of the mechanical properties of sandstone–coal–bolt specimens with different angles under conventional triaxial compression," *International Journal of Geomechanics*, vol. 21, no. 6, Article ID 4021067, 2021.

[2] H. Gao, Q. Wang, B. Jiang et al., "Relationship between rock uniaxial compressive strength and digital core drilling parameters and its forecast method," *International Journal of Coal Science & Technology*, vol. 8, no. 4, pp. 605–613, 2021.

[3] X. Zhao, H. Li, and S. Zhang, "Analysis of the spalling process of rock mass around a deep underground ramp based on numerical modeling and in-situ observation," *Geomatics, Natural Hazards and Risk*, vol. 11, no. 1, pp. 1619–1637, 2020.

[4] W. J. Yu, K. Li, Z. Liu, B. F. An, P. Wang, and H. Wu, "Mechanical characteristics and deformation control of surrounding rock in weakly cemented siltstone," *Environmental Earth Sciences*, vol. 80, no. 9, 2021.

[5] D. Cao, A. Wang, S. Ning et al., "Coalfield structure and structural controls on coal in China," *International Journal of Coal Science & Technology*, vol. 7, no. 2, pp. 220–239, 2020.

[6] Y. Tang, R. Li, and S. Wang, "Research progress and prospects of coal petrology and coal quality in China," *International Journal of Coal Science & Technology*, vol. 7, no. 2, pp. 273–287, 2020.

[7] ISRM, "Suggested method for determining point load strength," *International Journal of Rock Mechanics and Mining Sciences & Geomechanics Abstracts*, vol. 22, no. 2, pp. 51–60, 1985.

[8] X. Zhao and Y. Li, "Estimation of support requirement for a deep shaft at the Xincheng Gold Mine, China," *Bulletin of Engineering Geology and the Environment*, vol. 80, no. 9, pp. 6863–6876, 2021.

[9] D. V. Andrea, R. L. Fisher, and D. E. Fogelson, "Prediction of compression strength from other rock properties," *Colorado School of Mines Quarterly*, vol. 59, no. 4b, pp. 623–640, 1964.

[10] E. Broch and J. A. Franklin, "The point-load strength test," *International Journal of Rock Mechanics and Mining Sciences & Geomechanics Abstracts*, vol. 9, no. 6, pp. 669–676, 1972.

[11] ASTM International, "Standard test method for determination of the point load strength index of rock," ASTM, West Conshohocken, PA, USA, ASTM D5731-16, 2016.

[12] R. Ulusay, K. Türeli, and M. H. Ider, "prediction of engineering properties of a selected litharenite sandstone from its petrographic characteristics using correlation and multivariate statistical techniques," *International Journal of Rock*

*Mechanics and Mining Sciences & Geomechanics Abstracts*, vol. 32, no. 5, p. A221, 1995.

[13] Z. T. Bieniawski, "The point-load test in geotechnical practice," *Engineering Geology*, vol. 9, no. 1, pp. 1–11, 1975.

[14] E. Broch, "Estimation of strength anisotropy using the point-load test," *International Journal of Rock Mechanics and Mining Sciences & Geomechanics Abstracts*, vol. 20, no. 4, pp. 181–187, 1983.

[15] N. Brook, "The equivalent core diameter method of size and shape correction in point load testing," *International Journal of Rock Mechanics and Mining Sciences & Geomechanics Abstracts*, vol. 22, no. 2, pp. 61–70, 1985.

[16] M. Şahin, R. Ulusay, and H. Karakul, "Point load strength index of half-cut core specimens and correlation with uniaxial compressive strength," *Rock Mechanics and Rock Engineering*, vol. 53, no. 8, pp. 3745–3760, 2020.

[17] J. Fan, Z. Guo, Z. Tao, and F. Wang, "Method of equivalent core diameter of actual fracture section for the determination of point load strength index of rocks," *Bulletin of Engineering Geology and the Environment*, vol. 80, no. 6, pp. 4575–4585, 2021.

[18] S. Lei, H. P. Kang, and F. Q. Gao, "Point load strength test of fragile coal samples and predictive analysis of uniaxial compressive strength," *Coal Science and Technology*, vol. 47, no. 4, pp. 107–113, 2019.

[19] P. Sha, Q. T. Zhang, J. Lin, and F. Q. Wu, "In-situ estimation of uniaxial compressive strength of Igneous rock based on point load strength," *Rock and Soil Mechanics*, vol. S2, pp. 1–10, 2020.

[20] I. R. Forster, "The influence of core sample geometry on the axial point-load test," *International Journal of Rock Mechanics and Mining Sciences & Geomechanics Abstracts*, vol. 20, no. 6, pp. 291–295, 1983.

[21] D. K. Ghosh and M. Srivastava, "Point-load strength: an index for classification of rock material," *Bulletin of Engineering Geology and the Environment*, vol. 44, no. 1, pp. 27–33, 1991.

[22] K. T. Chau and R. H. C. Wong, "Uniaxial compressive strength and point load strength of rocks," *International Journal of Rock Mechanics and Mining Sciences & Geomechanics Abstracts*, vol. 33, no. 2, pp. 183–188, 1996.

[23] H. J. Smith, "The point load test for weak rock in dredging applications," *International Journal of Rock Mechanics and Mining Sciences*, vol. 34, no. 3-4, pp. 291–295, 1997.

[24] G. Tsiambaos and N. Sabatakakis, "Considerations on strength of intact sedimentary rocks," *Engineering Geology*, vol. 72, no. 3, pp. 261–273, 2004.

[25] V. Palchik and Y. H. Hatzor, "The influence of porosity on tensile and compressive strength of porous Chalks," *Rock Mechanics and Rock Engineering*, vol. 37, no. 4, pp. 331–341, 2004.

[26] T. N. Singh, A. Kainthola, and A. Venkatesh, "Correlation between point load index and uniaxial compressive strength for different rock types," *Rock Mechanics and Rock Engineering*, vol. 45, no. 2, pp. 259–264, 2012.

[27] M. Kohno and H. Maeda, "Relationship between point load strength index and uniaxial compressive strength of Hydrothermally Altered soft rocks," *International Journal of Rock Mechanics and Mining Sciences (Oxford, England: 1997)*, vol. 50, pp. 147–157, 2012.

[28] D. Li and L. N. Y. Wong, "Point load test on meta-sedimentary rocks and correlation to UCS and BTS," *Rock Mechanics and Rock Engineering*, vol. 46, no. 4, pp. 889–896, 2013.

[29] A. Kaya and K. Karaman, "Utilizing the strength conversion factor in the estimation of uniaxial compressive strength from the point load index," *Bulletin of Engineering Geology and the Environment*, vol. 75, no. 1, pp. 341–357, 2016.

[30] Q.-S. Liu, Y.-F. Zhao, and X.-P. Zhang, "Case study: using the point load test to estimate rock strength of tunnels constructed by a tunnel boring machine," *Bulletin of Engineering Geology and the Environment*, vol. 78, no. 3, pp. 1727–1734, 2019.

[31] Á. Rabat, M. Cano, R. Tomás, Á. E. Tamayo, and L. R. Alejano, "Evaluation of strength and deformability of soft sedimentary rocks in dry and saturated conditions through needle penetration and point load tests: a comparative study," *Rock Mechanics and Rock Engineering*, vol. 53, no. 6, pp. 2707–2726, 2020.

[32] Y. G. Xue, F. M. Kong, S. C. Li et al., "Using indirect testing methods to quickly acquire the rock strength and rock mass classification in tunnel engineering," *International Journal of Geomechanics*, vol. 20, no. 5, Article ID 5020001, 2020.

[33] W.-Q. Xie, X.-P. Zhang, Q.-S. Liu, S.-H. Tang, and W.-W. Li, "Experimental investigation of rock strength using Indentation test and point load test," *International Journal of Rock Mechanics and Mining Sciences*, vol. 139, Article ID 104647, 2021.

[34] S. Kahraman, "The determination of uniaxial compressive strength from point load strength for pyroclastic rocks," *Engineering Geology*, vol. 170, pp. 33–42, 2014.

[35] K. Diamantis, E. Gartzos, and G. Migiros, "Study on uniaxial compressive strength, point load strength index, dynamic and physical properties of serpentinites from Central Greece: test results and empirical relations," *Engineering Geology*, vol. 108, no. 3, pp. 199–207, 2009.

[36] I. Yilmaz, "A New testing method for indirect determination of the unconfined compressive strength of rocks," *International journal of rock mechanics and mining sciences (Oxford, England: 1997)*, vol. 46, no. 8, pp. 1349–1357, 2009.

[37] M. Heidari, G. R. Khanlari, M. Torabi Kaveh, and S. Kargarian, "Predicting the uniaxial compressive and tensile strengths of gypsum rock by point load testing," *Rock Mechanics and Rock Engineering*, vol. 45, no. 2, pp. 265–273, 2012.

[38] F. Kong and J. Shang, "A validation study for the estimation of uniaxial compressive strength based on index tests," *Rock Mechanics and Rock Engineering*, vol. 51, 2018.

[39] P. M. Santi, "Field methods for characterizing weak rock for engineering," *Environmental and Engineering Geoscience*, vol. 12, no. 1, pp. 1–11, 2006.

[40] L. Selçuk and H. Süleyman Gökçe, "Estimation of the compressive strength of concrete under point load and its approach to strength criterions," *KSCE Journal of Civil Engineering*, vol. 19, no. 6, pp. 1767–1774, 2015.

[41] R. Kallu and P. Roghanchi, "Correlations between direct and indirect strength test methods," *International Journal of Mining Science and Technology*, vol. 25, no. 3, pp. 355–360, 2015.

[42] A. Kılıç and A. Teymen, "Determination of mechanical properties of rocks using simple methods," *Bulletin of Engineering Geology and the Environment*, vol. 67, no. 2, pp. 237–244, 2008.

[43] S. L. Quane and J. K. Russell, "Rock strength as a metric of welding Intensity in pyroclastic deposits," *European Journal of Mineralogy*, vol. 15, no. 5, pp. 855–864, 2003.

[44] Ministry of Education of the People's Republic of China, "General rules for X-ray polycrystalline diffractometry,"

Ministry of Education of the People's Republic of China, Beijing, China, JY/T 0587-2020, 2020.

[45] American Society for Testing and Materials (Astm), "Annual book of ASTM standards," ASTM, Philadelphia, PA, USA, vol 04.08, 1994.